

Mid-infrared sources in the ELAIS Deep X-ray Survey

J.C. Manners¹, S. Serjeant^{2,3}, S. Bottinelli⁴, M. Vaccari^{1,2,5}, A. Franceschini¹,
I. Perez-Fournon⁶, E. Gonzalez-Solares⁷, C.J. Willott⁸, O. Johnson⁹, O. Almaini¹⁰,
M. Rowan-Robinson², S. Oliver¹¹

¹*Dipartimento di Astronomia, Università di Padova, Vicolo dell'Osservatorio 2, I-35122, Padova, Italy*

²*Astrophysics Group, Blackett Laboratory, Imperial College, Prince Consort Road, London SW7 2BW, UK*

³*Centre for Astrophysics and Planetary Science, School of Physical Sciences, University of Kent, Canterbury, Kent, CT2 7NR, UK*

⁴*Institute for Astronomy, University of Hawaii, 2680 Woodlawn Drive, Honolulu, HI 96822, USA*

⁵*CISAS "G. Colombo", Università di Padova, Via Venezia 15, I-35131, Padova, Italy*

⁶*Instituto de Astrofísica de Canarias, C/ Via Lactea, 38200 La Laguna, S/C de Tenerife, Spain*

⁷*Institute of Astronomy, Madingley Road, Cambridge, CB3 0HA, UK*

⁸*Herzberg Institute of Astrophysics, National Research Council, 5071 West Saanich Rd, Victoria, B.C. V9E 2E7, Canada*

⁹*Institute for Astronomy, University of Edinburgh, Royal Observatory, Blackford Hill, Edinburgh EH9 3HJ, UK*

¹⁰*School of Physics and Astronomy, University of Nottingham, University Park, Nottingham NG7 2RD, UK*

¹¹*Astronomy Centre, Department of Physics & Astronomy, University of Sussex, Brighton, BN1 9QJ, UK*

MNRAS in press

ABSTRACT

We present a cross-correlation of the European Large Area *ISO* survey (ELAIS) with the ELAIS Deep X-ray Survey of the N1 and N2 fields. There are 7 *Chandra* point sources with matches in the ELAIS Final Analysis $15\mu\text{m}$ catalogue, out of a total of 28 extragalactic *ISO* sources present in the *Chandra* fields. Five of these are consistent with AGN giving an AGN fraction of ~ 19 per cent in the $15\mu\text{m}$ flux range $0.8 - 6$ mJy. We have co-added the hard X-ray fluxes of the individually-undetected *ISO* sources and find a low significance detection consistent with star formation in the remaining population. We combine our point source cross-correlation fraction with the *XMM-Newton* observations of the Lockman Hole and *Chandra* observations of the Hubble Deep Field North to constrain source count models of the mid-infrared galaxy population. The low dust-enshrouded AGN fraction in ELAIS implied by the number of cross-identifications between the ELAIS mid-infrared sample and the *Chandra* point sources is encouraging for the use of mid-infrared surveys to constrain the cosmic star formation history, provided there are not further large undetected populations of Compton-thick AGN.

Key words: surveys - X-rays: general - X-rays: galaxies - galaxies: active - quasars: general

1 INTRODUCTION

Enormous progress has recently been made in resolving the sources that comprise the extragalactic hard X-ray background (e.g. Mushotzky *et al.* 2000, Cowie *et al.* 2002, Moretti *et al.* 2003). Studies are now focusing on characterising the nature of these sources through multi-waveband imaging and spectroscopy. Surveys with the *ISO* satellite have recently discovered strong evolution in the mid-infrared galaxy population (e.g. Elbaz *et al.* 1999, Serjeant *et al.* 2000, Chary & Elbaz 2001, Gruppioni *et al.* 2002) which is thought to be mainly due to a strongly evolving obscured cosmic star formation history (e.g. Aussel *et al.* 1999), al-

though there is also a contribution from dust-enshrouded AGN. Optical spectroscopic follow-ups of these samples are underway (e.g. La Franca *et al.* 2003, Gonzalez-Solares *et al.* 2004, Perez-Fournon *et al.* in preparation) but as the sources might not be optically-thin at optical wavelengths, nor emitting isotropically, it is possible that heavily dust-enshrouded populations may be mis-classified by this approach. The *Chandra* observations of the HDF-North (e.g. Hornschmeier *et al.* 2001, Alexander *et al.* 2002) placed constraints on the fraction of dust-enshrouded AGN at the faintest end of the $15\mu\text{m}$ source counts. Most of the known $15\mu\text{m}$ galaxies are at somewhat higher flux densities, however. Some

inroads were made on the AGN fraction for brighter mid-infrared sources by Alexander et al. (2001) using *BeppoSAX* observations of the ELAIS survey (described below), but the *BeppoSAX* depth was not sufficient to detect most Compton-thin Seyfert II galaxies in the targeted ELAIS field. Fadda et al. (2002) provided the first study with a reasonably significant number of sources with hard X-ray and mid-infrared emission. They combined *XMM-Newton* observations of the Lockman Hole and *Chandra* observations of the HDF-N with coincident ISOCAM data. This paper will provide further statistics using 2 *Chandra* pointings in the ELAIS northern survey regions N1 and N2. An upcoming analysis of the *Spitzer* Wide-area Infrared Extragalactic Survey (SWIRE, Lonsdale et al. 2003) observations in the N1 region will provide enhanced statistics in complementary wavebands.

The European Large Area *ISO* Survey, ELAIS, was the largest open time project on *ISO*, covering wavelengths from $6.7\mu\text{m}$ to $175\mu\text{m}$ (Oliver et al. 2000, Rowan-Robinson et al. 2004). The survey, and its follow-ups, have many ambitious aims, including tracing the cosmic star formation history to $z \sim 1$ and the discovery of ultra- and hyper-luminous galaxies at high redshift. The mid-infrared source counts (Serjeant et al. 2000, Gruppioni et al. 2002, Elbaz et al. in preparation) and far-infrared source counts (Efstathiou et al. 2000) both show evidence for strong evolution, as does the far-infrared luminosity function (Serjeant et al. 2001). The ELAIS mid-infrared source counts cover the transition from Euclidean slope to steep evolution; by virtue of the large area and large investment in observing time, ELAIS represents by far the largest sample of galaxies from this strongly evolving mid-infrared population. A high proportion have been revealed as ultra-luminous infrared galaxies (14% of $15\mu\text{m}$ galaxies with known z) including 9 hyper-luminous infrared galaxies (Morel et al. 2001, Rowan-Robinson et al. 2004).

Thanks to extensive multi-wavelength coverage, the ELAIS fields have now arguably become the most well studied regions of their size, and natural targets for on-going or planned large-area surveys with the most powerful ground and space-based facilities. Further details on ELAIS multi-wavelength observations and catalogues are presented in Rowan-Robinson et al. (2004). In particular, ELAIS $15\mu\text{m}$ observations will complement the SWIRE survey in three areas (N1, N2 and S1) by covering the 8-24 μm gap in *Spitzer*'s filters.

In the ELAIS Deep X-ray survey we made deep *Chandra* pointings of the ELAIS N1 and N2 fields to a limiting depth of $\sim 10^{-15} \text{ erg s}^{-1} \text{ cm}^{-2}$ in the 0.5 – 8keV band, with a total exposure of $\sim 75\text{ks}$ in each field. Manners et al. (2003) present the data and source counts. Gonzalez-Solares et al. (in preparation) present follow-up imaging and optical spectroscopy of the sample and Willott et al. (2003) present Subaru infrared spectroscopy. Almaini et al. (2003) present a cross-correlation of the *Chandra* sources with the sub-mm sources of Scott et al. (2002) and Fox et al. (2002), and measure the clustering of the *Chandra* population.

Here we present a cross-correlation of the *Chandra* X-ray sources with the mid-infrared sources from the ELAIS survey. Section 2 summarises the data acquisition in the mid-infrared and X-ray, and provides references to more exhaustive descriptions for the interested reader. Section 3 describes the cross-correlation between the *ISO* and *Chandra* data, and section 4 discusses the significance of the results.

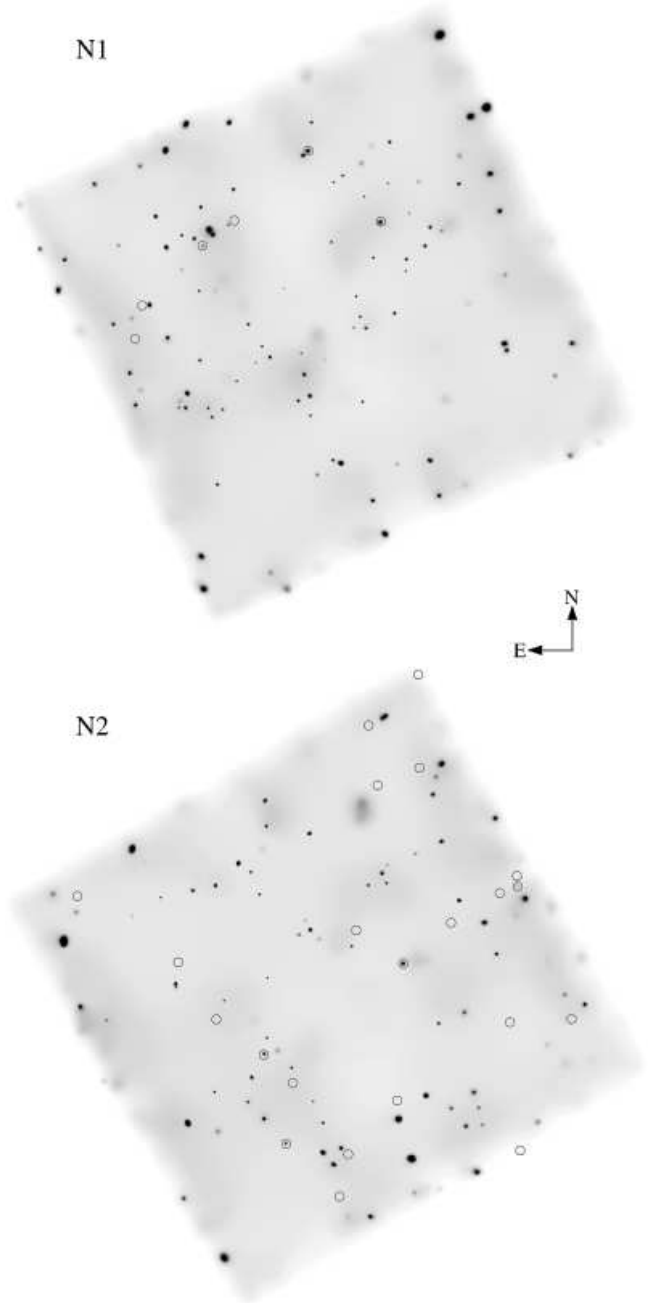


Figure 1. Positions of the 28 extragalactic $15\mu\text{m}$ *ISO* sources (black circles) superimposed on the smoothed 0.5 – 8 keV *Chandra* images. The images have been adaptively smoothed using the flux-conserving algorithm CSMOOTH from the *Chandra* Interactive Analysis of Observations (CIAO) package.

2 OBSERVATIONS

As part of ELAIS, ISOCAM observations were carried out covering 10.3 deg^2 at $15\mu\text{m}$. The observations were carried out in raster mode, with most of the survey area confined to three northern fields (N1: 2.67 deg^2 , N2: 2.67 deg^2 , N3: 0.88 deg^2) and one southern field (S1: 3.96 deg^2). Further details on the observation strategy can be found in Oliver et al. (2000).

Data reduction of ELAIS $15\mu\text{m}$ observations was re-

ID ¹	<i>Chandra</i> position ² (J2000.0)	<i>ISO</i> position ³ (J2000.0)	Offset ⁴ "	Prob. ⁵ ×10 ⁻³	f_X 0.5 - 8 keV ⁶ erg cm ⁻² s ⁻¹	$f_{15\mu m}$ ⁷ mJy	z ⁸	Class ⁹
N1_20	16:10:46.57+54:35:38.8	16:10:46.66+54:35:39.0	2.26	1.26	2.31×10^{-15}	1.844	0.0634	SB
N1_49	16:10:20.88+54:39:00.9	16:10:20.80+54:39:01.7	2.14	0.32	11.1×10^{-15}	2.918		AGN 2
N1_69	16:10:03.18+54:36:28.4	16:10:03.01+54:36:30.1	4.75	0.13	59.5×10^{-15}	1.453	0.2675	AGN 1
N2_25	16:36:55.79+40:59:10.5	16:36:55.83+40:59:09.2	1.46	0.12	10.2×10^{-15}	1.017	2.61	AGN 1 [‡]
N2_33	16:36:51.69+40:56:00.4	16:36:51.61+40:55:59.0	2.12	0.79	3.05×10^{-15}	1.732	0.4762	AGN 2 [‡]
N2_52	16:36:29.71+41:02:22.7	16:36:29.78+41:02:23.0	1.44	0.03	37.8×10^{-15}	1.009	0.02 [†]	AGN 1
N2_107	16:36:08.41+41:05:07.0	16:36:08.18+41:05:07.2	4.58	4.79	1.76×10^{-15}	8.935	0.1683	SB

Table 1. *Chandra* sources with ISOCAM 15 μm counterparts in the ELAIS regions N1 & N2. ¹*Chandra* source ID from Manners *et al.* (2003). ²Manners *et al.* (2003). ³Rowan-Robinson *et al.* (2004). ⁴Offset between *Chandra* and 15 μm *ISO* positions. ⁵Probability of this cross-correlation being a random association (see section 3). ⁶*Chandra* full band flux (Manners *et al.* 2003). ⁷ISOCAM 15 μm flux density (Rowan-Robinson *et al.* 2004). ⁸Spectroscopic redshifts ([†]photometric, 1 σ error \sim 0.1) reported in Rowan-Robinson *et al.* (2003). ⁹Likely object class as suggested by this paper (section 4.1) or [‡]previously confirmed by optical spectroscopy.

	N1_20	N1_49	N1_69	N2_25	N2_33	N2_52	N2_107
$f_{1.4GHz}$ ^a	0.26 ± 0.01	5.08 ± 0.01	0.15 ± 0.01	0.13 ± 0.01 ³	57.62 ± 0.02 ⁴		3.09 ± 0.02 ⁴
<i>ISO</i> $f_{175\mu m}$ ^a							803 ± 102
<i>IRAS</i> $f_{100\mu m}$ ^a							898 ± 126 ¹
<i>ISO</i> $f_{90\mu m}$ ^a							614 ± 37
<i>IRAS</i> $f_{60\mu m}$ ^a							351 ± 39 ¹
<i>ISO</i> $f_{15\mu m}$ ^a	1.84 ± 0.21	2.92 ± 0.27	1.45 ± 0.19	1.02 ± 0.14	1.73 ± 0.11	1.01 ± 0.14	8.94 ± 0.10
<i>ISO</i> $f_{6.7\mu m}$ ^a							2.30 ± 0.12
K 2.2 μm ^b	14.57 ± 0.08			19.1 ± 0.1 ³		13.04 ± 0.07	14.05 ± 0.12
H 1.65 μm ^b	14.87 ± 0.02 ²	16.41 ± 0.05 [†]	15.91 ± 0.03 ²	21.20 ± 0.03 ²	16.23 ± 0.03 ²	13.33 ± 0.05	14.61 ± 0.14
J 1.25 μm ^b					17.21 ± 0.13	13.99 ± 0.04	15.52 ± 0.13
i' 775nm ^b	16.64 ± 0.02 ²		17.86 ± 0.02 ²	22.55 ± 0.03 ²	18.15 ± 0.03 ²	15.01 ± 0.03 ²	16.56 ± 0.03 ²
r' 623nm ^b	17.12 ± 0.02 ²		18.46 ± 0.02 ²	22.95 ± 0.03 ²	19.39 ± 0.03 ²	15.68 ± 0.03 ²	17.25 ± 0.03 ²
g' 486nm ^b	17.68 ± 0.02 ²	23.88 ± 0.13 [†]	19.21 ± 0.02 ²	22.87 ± 0.03 ²	20.45 ± 0.03 ²	16.50 ± 0.03 ²	18.14 ± 0.03 ²
U 361nm ^b	17.61 ± 0.02 ²	23.78 ± 0.16 [†]	19.11 ± 0.03 ²	22.94 ± 0.03 ²	20.62 ± 0.03 ²	17.33 ± 0.03 ²	18.99 ± 0.03 ²
$f_{0.5-2keV}$ ^c	0.8 ± 0.3	1.0 ± 0.3	23.0 ± 1.2	2.1 ± 0.4	< 0.5	14.2 ± 1.0	1.0 ± 0.3
f_{2-8keV} ^c	< 2.4	22.1 ± 2.7	39.8 ± 3.5	14.7 ± 2.1	5.2 ± 1.4	26.0 ± 2.8	< 3.9
α_{IX}	1.53 ± 0.03	1.32 ± 0.01	1.20 ± 0.01	1.26 ± 0.02	1.41 ± 0.03	1.21 ± 0.02	1.70 ± 0.03
HR	-0.34 ± 0.24	0.69 ± 0.09	-0.40 ± 0.04	0.26 ± 0.11	0.37 ± 0.19	-0.38 ± 0.05	-0.26 ± 0.22

Table 2. Multi-waveband data for each cross-correlated source. Uncertainties are 1 σ . X-ray data are from Manners *et al.* (2003). Other waveband data are taken from Rowan-Robinson *et al.* (2004) except ¹Moshir *et al.* (1990), ²Gonzalez-Solares *et al.* (in preparation), ³Willott *et al.* (2003), ⁴Ciliegi *et al.* (1999), [†]aperture magnitudes provided by E. Gonzalez-Solares. Also included are the mid-IR to hard X-ray relation (α_{IX}) and the X-ray hardness ratio (HR) as defined in Manners *et al.* (2003). Units are ^amJy, ^bVega magnitudes, and ^c10⁻¹⁵ erg cm⁻² s⁻¹

cently completed by Vaccari *et al.* (in preparation). Data reduction was carried out using the LARI method (Lari *et al.* 2001, Lari *et al.* 2003), a new technique devised for the reduction of ISOCAM and ISOPHOT imaging data. Based on a physical model of the *ISO* detectors' behaviour, the method is particularly suited for the reliable detection of faint sources in *ISO* surveys, allowing sensitivity to be pushed to the instrumental limits.

A sample of 1056 sources (490 in N1 and 566 in N2) were detected with $S/N > 5$, spanning the 0.5 - 100 mJy flux range and thus filling the gap between the ISOCAM deep surveys (e.g. Elbaz *et al.* 1999) and the *IRAS* Faint Source Catalogue (Moshir *et al.* 1990).

The ELAIS Deep X-ray Survey was centred on regions in the ELAIS N1 and N2 fields selected to have low cirrus and HI column density (see Oliver *et al.* 2000 for more details). The *Chandra* observations are described in detail elsewhere (Manners *et al.* 2003), though we summarise the main

points here. The observations were taken with the *Chandra* ACIS (Advanced CCD Imaging Spectrometer) array. Integrations of 75ks were taken in each of N1 and N2. The pointing centroids are 16:10:20.11 +54:33:22.3 in N1 and 16:36:46.99 +41:01:33.7 in N2, with an area of 16.9' × 16.9' covered by the ACIS-I chips in each case, giving a total area of 571 sq. arcmin. The limiting flux levels are 4.6×10^{-16} erg s⁻¹ cm⁻² in the 0.5 - 2 keV band, and 2.2×10^{-15} erg s⁻¹ cm⁻² in the 2 - 8 keV band. The N1 region contains 125 *Chandra* sources from the 4 ACIS-I chips and 5 from the ACIS-S2 chip. The N2 region has 99 sources on the ACIS-I chips and 4 on the ACIS-S2 chip. Only sources from the ACIS-I chips were used for this analysis due to the poor resolution of the off-axis ACIS-S chips.

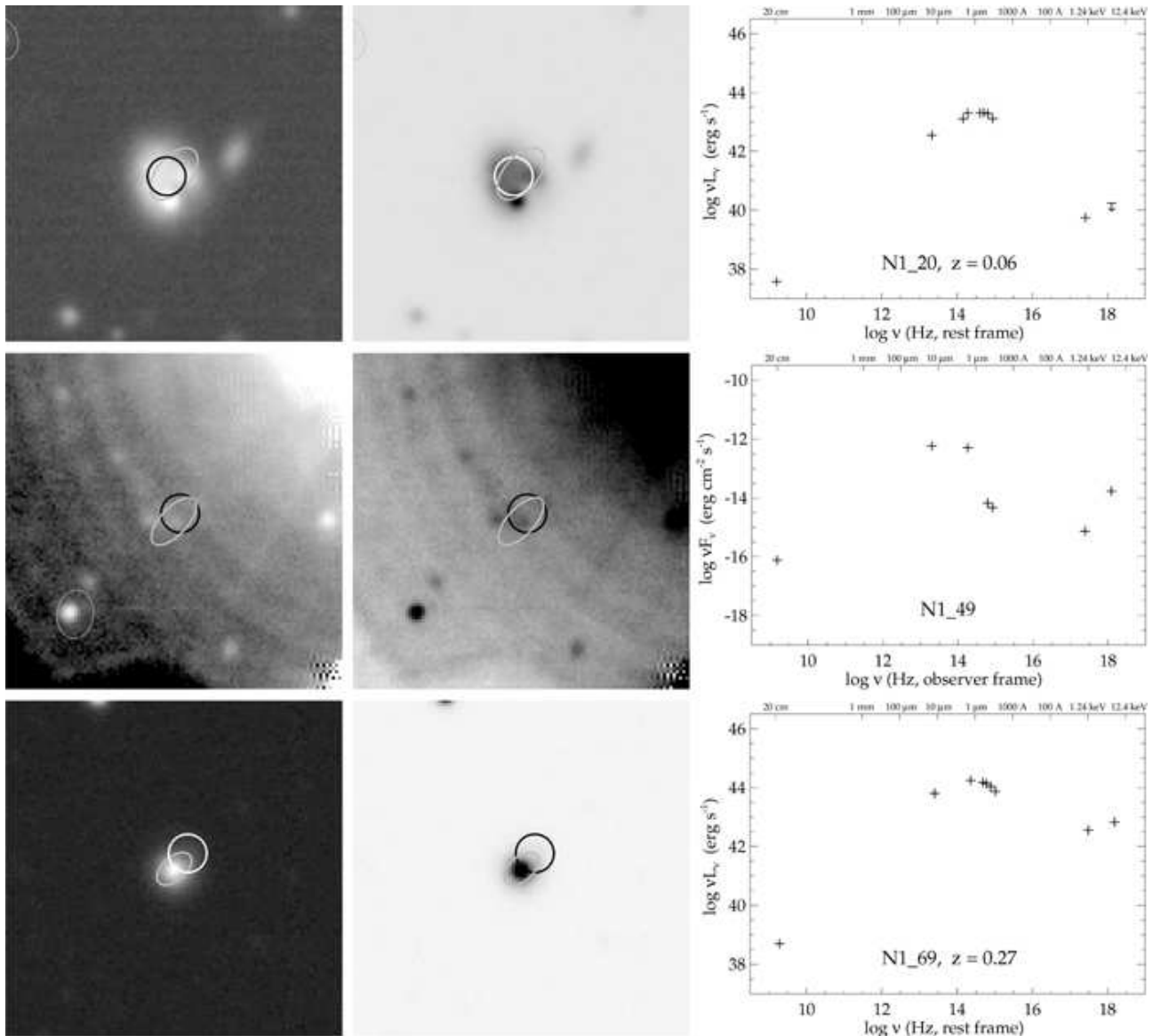


Figure 2. *Chandra* sources with a $15 \mu\text{m}$ counterpart in the N1 region. $25'' \times 25''$ r' -band postage stamps are from a 5400 second exposure with the INT WFC and are displayed in positive and negative grey-scale for clarity. Black or white circles indicate position of the *ISO* source and grey ellipses give the 3σ size of the X-ray PSF. Spectral energy distributions are at rest-frame wavelengths and displayed in units of luminosity where redshifts are available.

3 POSITIONAL CORRELATION BETWEEN THE *CHANDRA* AND *ISO* SOURCES

In the N1 region there are 9 $15\mu\text{m}$ Final Analysis ELAIS sources within the *Chandra* region, three of which are identified with stars and the remainder of which are galaxy IDs. In the N2 region there are 24 $15\mu\text{m}$ sources, two of which are identified with stars and the rest with galaxies or blank fields in the r' band image. The positions of the 28 extragalactic sources are plotted in Fig. 1 superimposed on the smoothed *Chandra* images.

We performed a simple near-neighbour search to cross-correlate the extragalactic *Chandra* and *ISO* sources within the area of the *Chandra* ACIS-I chips, using a $5''$ search radius. Astrometric 1σ errors for the *Chandra* sources are $\sim 1''$ (Manners *et al.* 2003), while the nominal astrometric

accuracy for the ELAIS $15 \mu\text{m}$ FA catalogue sources ranges from $\sim 0.8''$ to $2.0''$ (Vaccari *et al.* in preparation). The search radius of $5''$ was chosen as the approximate sum of the 2σ astrometric errors. Three matches were found in the N1 region and four in the N2 region (table 1, Fig. 1). All seven matches are with high reliability *ISO* sources (5σ).

To ensure the associations were real we calculated the probability of a random association between each mid-IR source and its X-ray counterpart. Following Fadda *et al.* (2002), we assume the X-ray counterpart belongs to a Poissonian distributed population so that

$$P = 1 - e^{-N(>S)\pi d^2} \quad (1)$$

where P is the probability of a random association within an offset distance d . $N(>S)$ is the number density of sources with flux greater than the possible X-ray counterpart (S).

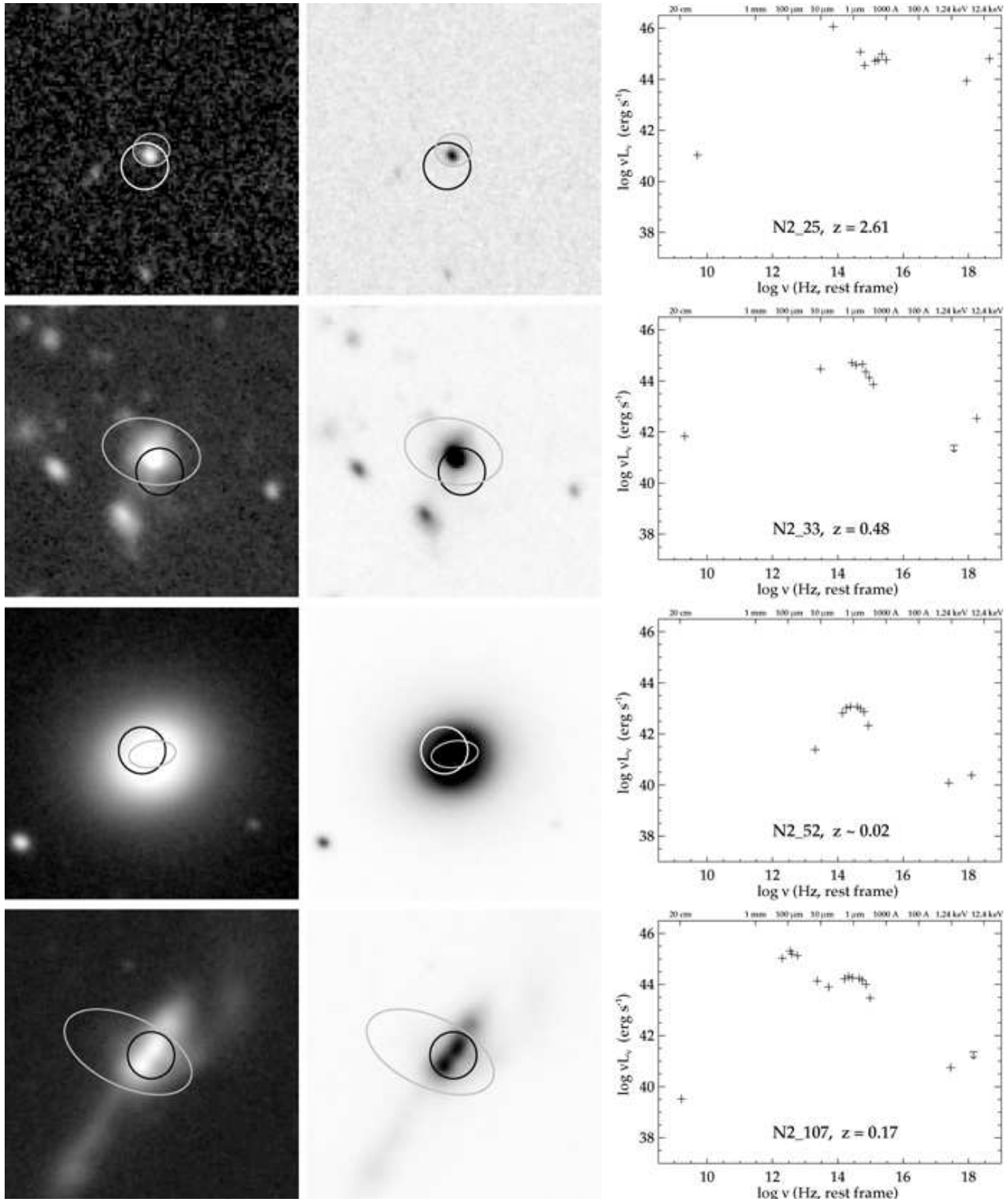


Figure 3. *Chandra* sources with a $15\ \mu\text{m}$ counterpart in the N2 region. $25'' \times 25''$ r' -band postage stamps are from a 7800 second exposure with the WHT and are displayed in positive and negative grey-scale for clarity. Black or white circles indicate position of the *ISO* source and grey ellipses give the 3σ size of the X-ray PSF. Spectral energy distributions are at rest-frame wavelengths and displayed in units of luminosity.

We calculate this probability for each source (table 1) with reference to the $\log(N)$ - $\log(S)$ relation for these regions (Manners *et al.* 2003). The chances of random associations are found to be very low.

Figs. 2 & 3 display the cross-correlations overlaid on optical postage stamps.

4 RESULTS AND DISCUSSION

4.1 Identifications

Properties of the 7 cross-correlated sources are reported in table 1. Multi-waveband data are reported and referenced in table 2. Also reported in table 2 are the mid-infrared to X-ray spectral indices (α_{IX} , described in section 4.2) and the X-ray hardness ratios (HR, from Manners *et al.* 2003). r' band postage stamps to a depth of $r' \sim 26$ are shown in Figs. 2 & 3 together with the spectral energy distribution (SED) of each source. For the 6 sources with available redshifts, SEDs are displayed in the rest frame in units of luminosity assuming a cosmology with $\Omega_\Lambda = 0.73$, $\Omega_M = 0.27$, and $H_0 = 71 \text{ km s}^{-1} \text{ Mpc}^{-1}$. For the source without a redshift (N1_49), the SED is displayed in the observed frame in units of flux. In order to derive flux densities for the SEDs, magnitudes were converted using the following zero points for each photometric band: K 657 Jy; H 1020 Jy; J 1600 Jy; i' 2491 Jy; r' 3133 Jy; g' 3876 Jy; U 1810 Jy. Flux densities at 1 keV and 5 keV were derived from the 0.5 - 2 keV and 2 - 8 keV *Chandra* bands respectively, assuming a power-law spectrum with photon index $\Gamma = 1.7$ within each band. A description follows of the properties and most probable identifications for each source:

N1_20 (CXOEN1 J161046.5+543538) A complex r' band morphology indicative of a recent merger. This low redshift ($z = 0.0634$) object has a soft X-ray spectrum and is below the detection threshold in the 2 - 8 keV band image. The mid-infrared to X-ray spectral index is also quite steep ($\alpha_{IX} = 1.51$). These characteristics are consistent with identification as a starburst galaxy (SB, table 1).

N1_49 (CXOEN1 J161020.8+543900) Spectroscopic identification of this object is hampered by the presence of a nearby bright star (as can be seen in the r' band postage stamp). No redshift is available, however a very hard X-ray spectrum combined with a relatively flat mid-infrared to X-ray spectral index indicates likely identification with an AGN. The X-ray spectrum is consistent with an apparent absorbing column of $N_H \sim 6 \pm 2 \times 10^{22} \text{ cm}^{-2}$ (assuming an underlying power law of $\alpha = 0.7$ and $z = 0$). Depending on the redshift of this source the actual N_H is likely to be higher with apparent absorbing column scaling as $(1+z)^{2.6}$. The mid-infrared to X-ray spectral index ($\alpha_{IX} = 1.32$) is also consistent with an absorbed AGN (see section 4.2). Given an AGN 2 classification in table 1.

N1_69 (CXOEN1 J161003.1+543628) Spectroscopic redshift of 0.2675. The flat mid-infrared to X-ray spectral index, luminosity and X-ray hardness ratio are all typical of a Seyfert galaxy (AGN 1, table 1).

N2_25 (CXOEN2 J163655.7+405910)

Spectroscopically confirmed quasar at a redshift of 2.61 (AGN 1, table 1). Its properties are extensively reported in Willott *et al.* (2003).

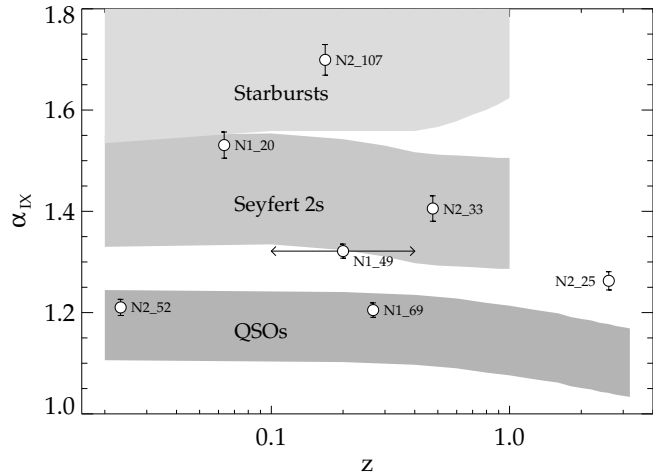


Figure 4. Mid-infrared to hard X-ray spectral indices (α_{IX}) vs. redshift. Shaded areas represent the error boxes for template SEDs of QSOs, Seyfert 2s and Starburst galaxies as reported in Alexander *et al.* (2001, Fig. 7). cf. Fadda *et al.* (2002, Fig. 8).

N2_33 (CXOEN2 J163651.6+405600)

Spectroscopically identified as a Seyfert 2 galaxy at a redshift of 0.4762 (AGN 2, table 1). The r' band image indicates an interaction is occurring with a smaller neighbour. Radio morphology suggests this to be an FR-II type AGN.

N2_52 (CXOEN2 J163629.7+410222) Elliptical galaxy with no obvious point-like nuclear source. A photometric redshift of ~ 0.02 suggests an X-ray luminosity that is low for an active galaxy ($1 \times 10^{40} \text{ erg s}^{-1}$ at 1 keV, $2 \times 10^{40} \text{ erg s}^{-1}$ at 5 keV). However, mid-infrared to X-ray spectral index and X-ray hardness ratio are both consistent with an AGN (AGN 1, table 1).

N2_107 (CXOEN2 J163608.4+410507) Interesting r' band morphology displaying merging galaxies with a double nucleus. Spectroscopic redshift of 0.1683. The X-ray spectrum is soft and of low-luminosity ($6 \times 10^{40} \text{ erg s}^{-1}$ at 1 keV) with the source undetected in the 2 - 8 keV band image. The relatively luminous infra-red spectrum supports identification with a starburst galaxy (SB, table 1).

Of the 7 matched sources, 1 is a spectroscopically confirmed quasar, 1 is spectroscopically identified as a Seyfert 2, a further 3 display properties of AGN, and 2 have properties consistent with starburst galaxies.

4.2 The mid-infrared to X-ray spectral indices

Values for the mid-infrared to X-ray spectral index (α_{IX}) are calculated using the flux density observed at $15\mu\text{m}$ and 5 keV, assuming a power-law spectrum of the form $F_\nu \propto \nu^{-\alpha_{IX}}$. The flux density at 5 keV is calculated from flux in the 2 - 8 keV *Chandra* band. For the 2 objects undetected in this band, the full 0.5 - 8 keV band is used.

The mid-infrared to X-ray spectral index can be a useful indicator to distinguish between AGN and starburst galaxies (e.g. Alexander *et al.* 2001, Fadda *et al.* 2002). Starburst galaxies are found to have high values of α_{IX} , while type-1 AGN have low values ($\alpha_{IX} < 1.2$). Type-2 AGN have values in between depending on the amount of obscuration. Fig. 4 plots the α_{IX} values for our 6 matched sources with

available redshifts. The figure displays values of α_{IX} as a function of redshift for template SEDs compiled by Alexander *et al.* (2001). Source N2_33, spectroscopically identified as a Seyfert 2 lies squarely within the region of the Seyfert 2 templates. N2_25, spectroscopically identified as a QSO has a value slightly higher than the QSO templates although still lower than expected for a Seyfert 2. Of the remaining objects studied here, N1_69 and N2_52 lie in the region of type-1 AGN, N1_20 and N2_107 are consistent with starbursts or highly obscured AGN, and N1_49 is consistent with a type-2 AGN.

4.3 Constraints on models of mid-infrared source counts

In the N1 region there are 6 extragalactic $15\mu\text{m}$ Final Analysis ELAIS sources within the *Chandra* region. In the N2 region conversely there are 22 extragalactic $15\mu\text{m}$ sources. The *Chandra* N2 region falls within an area of repeated *ISO* observations while the *Chandra* N1 region does not. The difference in source counts, however, is larger than expected and may indicate clustering on scales larger than the field size. This highlights the need for larger areas to be surveyed before sufficient count statistics can be gained. Here we consider our results along with number counts from the Hubble Deep Field - North (HDF-N) and the Lockman Hole (Fadda *et al.* 2002) in order to provide a comparison with recent models of mid-infrared source counts.

The $15\mu\text{m}$ flux range 0.8–6.0 mJy is well covered by the *ISO* observations in our *Chandra* regions. In this flux range there are 26 extragalactic $15\mu\text{m}$ sources in our sample. We take 5 of these objects to contain evidence of AGN from the *Chandra* and multi-waveband data. This gives an AGN fraction of 5/26 extragalactic sources, or 0.19 ± 0.09 over the given flux range, in a total area of ~ 571 sq. arcmin. This fraction will be a lower limit if any heavily obscured, Compton-thick AGN are present in our sample.

Fadda *et al.* (2002) report AGN number counts for mid-infrared sources in the Lockman Hole and HDF-N. They find for the Lockman Hole an AGN fraction of 13/103 extragalactic sources (0.13 ± 0.04) within the $15\mu\text{m}$ flux range 0.5–3.0 mJy in a total area of 218 sq. arcmin. For the HDF-N the AGN fraction is 5/42 (0.12 ± 0.05) over a $15\mu\text{m}$ flux range of 0.1–0.5 mJy in a total area of 24.3 sq. arcmin.

We compare these results with models for the AGN contribution to mid-infrared surveys by Pearson (2001) and King & Rowan-Robinson (2003). These models primarily attempt to model the star formation history by fitting infrared source count observations with contributions from normal galaxies, starbursts, ultra-luminous infrared galaxies (ULIRGs) and AGN. The Pearson (2001) model uses local luminosity functions and pure luminosity evolution to describe the normal galaxy, starburst and AGN populations while the ULIRG component is evolved in both density and luminosity. The $15\mu\text{m}$ and $850\mu\text{m}$ source counts are used to constrain the model. The best fit to the observations is obtained where the ULIRG component undergoes two major phases of evolution, rapid merging to $z \sim 1$ and an exponential evolution in luminosity to higher redshifts. This has an effect on the AGN fraction of the source counts which will be tested here. The King & Rowan-Robinson (2003) models are updated versions of models developed by Rowan-

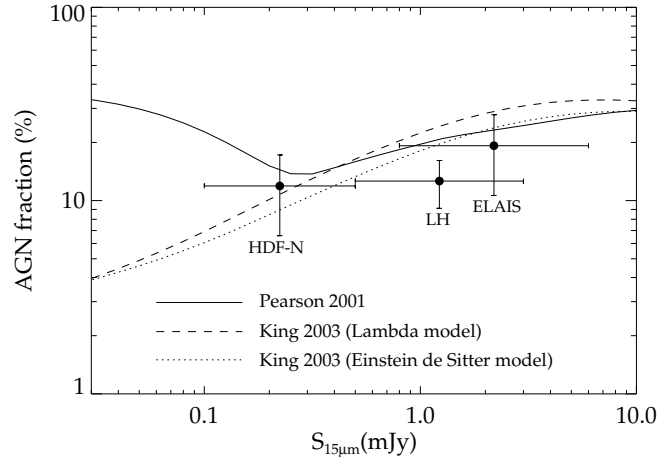


Figure 5. AGN fraction in the mid-infrared population derived from the ELAIS Deep X-ray survey (this work), as well as fractions derived by Fadda *et al.* (2002) from *Chandra* observations of the Hubble Deep Field North (HDF-N) and *XMM-Newton* observations of the Lockman Hole (LH). Also plotted are the predictions from the integral counts of Pearson (2001), and two models from King & Rowan-Robinson (2003) (based on the models of Rowan-Robinson 2001).

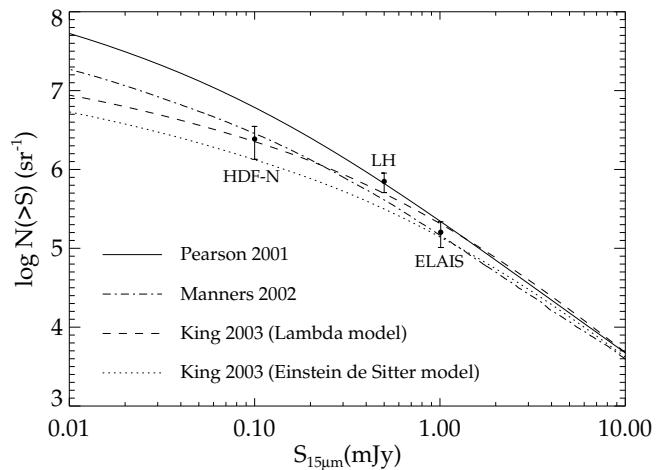


Figure 6. Integral AGN number counts for $15\mu\text{m}$ surveys. Values for the Lockman Hole and HDF-N are taken from Fadda *et al.* (2002). Number count predictions are taken from the same models displayed in Fig. 5, plus that of Manners (2002).

Robinson (2001) and are calculated for lambda and Einstein de Sitter cosmologies. They allow for both density and luminosity evolution in all four populations. The AGN contribution in both models is found using a $12\mu\text{m}$ luminosity function from Rush, Malkan & Spinoglio (1993) which does not include Compton-thick AGN and can therefore be directly compared with these observations. Fig. 5 displays the AGN fraction predicted by these models against source flux. All 3 models shown are consistent with AGN fractions reported here for the ELAIS regions and for the HDF-N. The AGN fraction in the Lockman Hole is slightly lower than the predictions of these models.

We also compare the observations to modelled predictions for the cumulative AGN source counts at $15\mu\text{m}$ (Fig. 6). To make a reliable comparison it was necessary

to correct our AGN source counts for completeness. While the 15 μm data reduction has been completed by Vaccari *et al.* (in preparation), completeness estimates are to be published in Lari *et al.* (in preparation) and are not yet available. Therefore, values from Gruppioni *et al.* (2002) were taken as representative. By estimating the completeness at the flux level of our sources we calculate the expected number of AGN above the flux limit to be ~ 7.7 (ELAIS data point, Fig. 6). We can now compare a further model from Manners (2002) which assumes AGN are responsible for the entire hard X-ray background and predicts the emission of these AGN in the mid-infrared. Observations in the HDF-N agree with models by King & Rowan-Robinson (2003) and Manners (2002), while the Pearson (2001) model over-predicts the number of sources at this depth. AGN counts from the Lockman Hole are consistent with the Pearson (2001) and King & Rowan-Robinson (2003, Lambda) models, whilst the AGN counts reported here for the ELAIS survey agree well with all the model predictions.

4.4 Statistical hard X-ray limits of ELAIS ISO sources

One further method of constraining the source count models is the statistical detection of *ISO* sources in the *Chandra* map. By co-adding the *Chandra* fluxes at the positions of *ISO* sources not detected individually, we can obtain a constraint on the mean hard X-ray flux and hard X-ray to mid-infrared flux ratio for the remaining population.

In the N1 region there are 3 extragalactic sources undetected by *Chandra* whilst in the N2 region there are 18 (see Fig. 1). In order to obtain limits on the X-ray flux for these sources it was necessary to define source regions on the *Chandra* images. These regions were positioned accurately using the astrometry obtained by cross-correlating *Chandra* and *r'*-band sources (Manners *et al.* 2003). The size of each region was defined as a circle containing 95% encircled energy for a monoenergetic *Chandra* PSF at 4.51 keV at the relevant source position.

For each field, around 6 circular background regions of radii ranging from $\sim 1' - 2'$ were selected. These were chosen carefully to avoid contamination from known *Chandra* sources and to cover regions of typical effective exposure. The background counts expected in each source region were then calculated by correcting for the difference in effective exposure. This method was preferred over the use of individual local background estimates due to the slow change in background counts over the image and the better statistics gained from using the larger background regions.

Counts were extracted from the hard (2 - 8 keV) and soft (0.5 - 2 keV) band *Chandra* images. Source regions were individually corrected for effective exposure, background subtracted, and then co-added to obtain an estimate of the total flux.

In the hard band we obtain a total of 58 counts with 49.3 background counts expected. The Poisson probability of obtaining 58 or more counts with 49.3 expected is 0.123, equivalent to a tentative detection at a confidence level of 87.7%. This is equivalent to a mean flux of $2.2 \pm 1.5 \times 10^{-16}$ erg cm $^{-2}$ s $^{-1}$ for each of the 21 sources. In the soft band we obtain a total of 43 counts with 24.1 background counts expected. The Poisson probability of obtaining 43 or more

counts with 24.1 expected is 3×10^{-4} , equivalent to a reliable detection at a confidence level of 99.97%. These counts are equivalent to a mean flux of $6.7 \pm 2.5 \times 10^{-17}$ erg cm $^{-2}$ s $^{-1}$.

In order to check the validity of the stacking analysis we repeated the procedure with the positions randomised over the areas of the *Chandra* field that are free of known sources. This was repeated 10 times for each band. The distributions of the counts obtained were consistent with a Gaussian of mean and variance equal to the expected number of background counts in each case.

The stronger detection in the soft band is indicative of the higher efficiency of *Chandra* in this band and does not imply these sources have a particularly soft X-ray spectrum. The hardness ratio (defined in Manners *et al.* 2003) for the co-added regions is -0.09 ± 0.38 , somewhat harder than expected for starbursts. However, the low significance of the hard X-ray detection means this must be used with caution.

Seven of the unmatched sources have spectroscopic redshifts available, ranging from $z = 0.10$ to 0.24. At a typical redshift of 0.2 the mean fluxes given above would equate to luminosities of 5.4×10^{39} at 1 keV and 1.9×10^{40} at 5 keV. This is entirely consistent with a starburst origin for the X-ray emission. The mean 15 μm flux for the 21 unmatched sources is 1.489 mJy. This leads to a mean spectral index of $\alpha_{IX} = 1.68$, also consistent with purely starburst galaxies.

It should be noted that 'Compton thick' AGN will not appear in the X-ray data and constitute an unknown fraction of the unmatched sources.

4.5 The cosmic star formation history from mid-infrared flux limited samples

Of the sources detected in field surveys by the *ISO* satellite, by far the largest fraction and largest number of moderate-redshift ($z > 0.5$) systems are found in mid-infrared ISO-CAM surveys, as opposed to the far-infrared (90 - 175 μm) surveys conducted by the ISOPHOT instrument. Also, the surveys now being performed by the *Spitzer* satellite, such as SWIRE (Lonsdale *et al.* 2003), will have high-redshift objects preferentially detected in the mid-infrared passbands. The AGN torus emission peaks in the infrared (e.g. Haas *et al.* 1998) so it might be expected that a large population of AGN would occur in these surveys in addition to high- z star forming galaxies. Our AGN fractions, together with other studies (Fadda *et al.* 2002, Alexander *et al.* 2002), show this population to be a fairly well-determined minority and are encouraging for the use of mid-infrared samples for constraining the cosmic star formation history. The mid-infrared luminosity is a reasonably good star formation rate indicator, albeit affected by complicated K-correction effects (e.g. Xu *et al.* 1998).

The main caveat is that our *Chandra* data still do not exclude the possibility of a large population of Compton-thick objects at moderate redshifts ($z \sim 1$). Alexander *et al.* (2002), however, argue that this fraction should be low. They performed an X-ray stacking analysis on those infrared galaxies that were not clearly AGN at X-ray energies but were still individually detected in the 1 Ms *Chandra* Deep Field North Survey. They find an average X-ray spectral slope of $\Gamma = 2.0$, indicating a low contribution from the much flatter spectra of obscured AGN.

5 CONCLUSIONS

We performed a cross-correlation of X-ray and mid-infrared point sources in the ELAIS N1 and N2 fields, using data from the *Chandra* and *ISO* satellites. 7 extragalactic matches are found (out of a total of 28 *ISO* sources) within the area of the *Chandra* ACIS-I chips. 2 of these are spectroscopically identified as AGN. Based on X-ray to IR flux ratios, X-ray hardness ratios, and luminosities, 3 of the remaining 5 are also consistent with AGN while the other 2 are consistent with starburst galaxies. This provides an AGN fraction of ~ 19 per cent in the $15\mu\text{m}$ flux range $0.8 - 6$ mJy. We have co-added the hard X-ray flux at the positions of the 21 undetected *ISO* sources providing only a 1.4 sigma detection. This translates to a mean hard X-ray to mid-IR flux ratio consistent with star formation in these objects. Our cross-correlations, when compared with *XMM-Newton* observations of the Lockman Hole and *Chandra* observations of the northern Hubble Deep Field, allow us to place constraints on source count models of the $15\mu\text{m}$ source population. The AGN fractions and number counts are broadly consistent with models by Pearson (2001) and King & Rowan-Robinson (2003). We argue our data is encouraging for the use of mid-infrared samples to constrain the cosmic star formation history, provided there is not a large contribution from Compton-thick AGN.

ACKNOWLEDGEMENTS

This research has made use of the NASA Extra-galactic Database (NED), operated by the Jet Propulsion Laboratory, California Institute of Technology, under contract with the National Aeronautics and Space Administration. This work was partly funded under PPARC grant number GR/K98728. JCM would like to thank the referee for detailed and useful comments.

REFERENCES

- Alexander D.M., La Franca F., Fiore F., Barcons X., et al. 2001, *ApJ*, 554, 18
- Alexander D.M., Aussel H., Bauer F.E., Brandt W.N., et al. 2002, *ApJ*, 568, L85
- Almaini O., Scott S.E., Dunlop J.S., Manners J.C., et al. 2003, *MNRAS*, 338, 303
- Aussel H., Vigroux L., Franceschini A., Elbaz D., et al. 1999, *AAS*, 195, 0917
- Chary R. & Elbaz D. 2001, *ApJ*, 556, 562
- Ciliegi P., McMahon R.G., Miley G., Gruppioni C., et al. 1999, *VizieR Online Data Catalog*, 730, 20222
- Comastri A., Mignoli M., Ciliegi P., Severgnini P., et al. 2002, *ApJ*, 571, 771
- Cowie L.L., Garmire G.P., Bautz M.W., Barger A.J., et al. 2002, *ApJ*, 566, L5
- Elbaz D., Cesarsky C.J., Fadda D., Aussel H., et al. 1999, *A&A*, 351, L37
- Efstathiou A., Oliver S., Rowan-Robinson M., Surace C. 2000, *MNRAS*, 319, 1169
- Fadda D., Flores H., Hasinger G., Franceschini A., et al. 2002, *A&A*, 383, 838
- Fox M.J., Efstathiou A., Rowan-Robinson M., Dunlop J.S., et al. 2002, *MNRAS*, 331, 839
- Gonzalez-Solares E.A., Perez-Fournon I., Rowan-Robinson M., Oliver S., et al. 2004 *MNRAS* submitted, astro-ph/0402406
- Gruppioni C., Lari C., Pozzi F., Zamorani G., et al. 2002, *MNRAS*, 335, 831
- Haas M., Chini R., Meisenheimer K., Stickel M., et al. 1998, *ApJ*, 503, L109
- Hornschemeier A.E., Brandt W.N., Garmire G.P., Schneider D.P., et al. 2001, *ApJ*, 554, 742
- King A.J. & Rowan-Robinson M. 2003, *MNRAS*, 339, 260
- La Franca F., Gruppioni C., Matute I., Pozzi F., et al. 2003, *AJ* submitted
- Lari C., Pozzi F., Gruppioni C., Aussel H., et al. 2001, *MNRAS*, 325, 1173
- Lari C., Vaccari M., Rodighiero G., Fadda D., et al. 2003, *ESA SP-511: Exploiting the ISO Data Archive. Infrared Astronomy in the Internet Age*, 349
- Lonsdale C.J., Smith H.E., Rowan-Robinson M., Surace J., et al. 2003, *PASP*, 115, 897
- Manners J.C. 2002, Ph.D. thesis, University of Edinburgh
- Manners J.C., Johnson O., Almaini O., Willott C.J., et al. 2003, *MNRAS*, 343, 293
- Morel T., Efstathiou A., Serjeant S., Marquez I. 2001, *MNRAS*, 327, 1187
- Moretti A., Campana S., Lazzati D., Tagliaferri G. 2003, *ApJ*, 588, 696
- Moshir M., Kopan G., Conrow T., McCallon H., et al. 1990, *IRAS Faint Source Catalogue*, version 2.0
- Mushotzky R.F., Cowie L.L., Barger A.J., & Arnaud K.A. 2000, *Nature*, 404, 459
- Oliver S., Rowan-Robinson M., Alexander D.M., Almaini O., et al. 2000, *MNRAS*, 316, 749
- Pearson C.P. 2001, *MNRAS*, 325, 1511
- Rowan-Robinson M. 2001, *ApJ*, 549, 745
- Rowan-Robinson M., Lari C., Perez-Fournon I., Gonzalez-Solares E.A., et al. 2004, *MNRAS* 351, 1290
- Rush B., Malkan M.A., & Spinoglio L. 1993, *ApJS*, 89, 1
- Scott S.E., Fox M.J., Dunlop J.S., Serjeant S., et al. 2002, *MNRAS*, 331, 817
- Serjeant S., Oliver S., Rowan-Robinson M., Crockett H., et al. 2000, *MNRAS*, 316, 768
- Serjeant S., Efstathiou A., Oliver S., Surace C. 2001, *MNRAS*, 322, 262
- Willott C.J., Simpson C., Almaini O., Manners J.C., et al. 2003, *MNRAS*, 339, 397
- Xu C., Hacking P.B., Fang F., Shupe D.L., et al. 1998, *ApJ*, 508, 576